

Variability, Petrography and Provenance of Basement Clasts in Core from CRP-2/2A, Victoria Land Basin, Antarctica

F. TALARICO^{1*}, S. SANDRONI¹, C. FIELDING² & C. ATKINS³

¹Dipartimento di Scienze della Terra, Università di Siena, via delle Cerchia 3, 53100 Siena - Italy

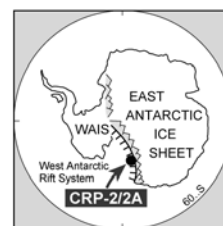
²Department of Earth Sciences, University of Queensland, Brisbane, QLD 4072 - Australia

³School of Earth Sciences, Victoria University of Wellington, P O Box 600, Wellington - New Zealand

*Corresponding author (talarico@unisi.it)

Received 27 July 1999; accepted in revised form 9 February 2000

Abstract - Distribution patterns, petrography, whole-rock and mineral chemistry, and shape and fabric data are described for the most representative basement lithologies occurring as clasts (granule to boulder grain-size class) from the 625 m deep CRP-2/2A drillcore. A major change in the distribution pattern of the clast types occurs at *c.* 310 mbsf, with granitoid-dominated clasts above and mainly dolerite clasts below; moreover, compositional and modal data suggest a further division into seven main detrital assemblages or petrofacies. In spite of this variability, most granitoid pebbles consist of either pink or grey biotite±hornblende monzogranites. Other less common and ubiquitous lithologies include biotite syenogranite, biotite-hornblende granodiorite, tonalite, monzogranitic or monzonitic porphyries (very common below 310 mbsf), microgranite, and subordinately, monzogabbro, Ca-silicate rocks, biotite-clinozoisite schist and biotite orthogneiss (restricted to the pre-Pliocene strata). The ubiquitous occurrence of biotite±hornblende monzogranite pebbles in both the Quaternary-Pliocene and Miocene-Oligocene sections, apparently reflects the dominance of these lithologies in the onshore basement, and particularly in the Cambro-Ordovician Granite Harbour Igneous Complex which forms the most extensive outcrop in southern Victoria Land. The petrographical features of the other CRP-2/2A pebble lithologies are consistent with a supply dominantly from areas of the Transantarctic Mountains facing the CRP-2/2A site, and they thus provide further evidence of a local provenance for the supply of basement clasts to the CRP-2/2A sedimentary strata.



INTRODUCTION

Drilling at CRP-2/2A provided a more or less continuous core through *c.* 625 m of Quaternary-Pliocene and Lower Miocene-Oligocene sedimentary strata on the margin of the Victoria Land Basin, in McMurdo Sound between the Transantarctic Mountains of South Victoria Land and the recent (5 Ma) volcanic Ross Island (Cape Roberts Science Team, 1999). CRP-2/2A was sited 14.2 km E of Cape Roberts, *c.* 900 m inboard of CRP-1, the first drillsite of the Cape Roberts Project (Cape Roberts Science Team, 1998a, 1998b, 1998c, 1998d). The background and objectives of the project, as well as the stratigraphy and chronology, and the climatic, depositional and tectonic aspects of the recovered strata are reported and described in Cape Roberts Science Team (1999). This paper presents distribution data on the clast population throughout the core, and petrographical, whole-rock and mineral chemistry data on the most representative plutonic and metamorphic lithologies occurring as clasts (pebble grain-size class) from the CRP-2/2A drillcore. It also includes comment on shape and fabric analysis of selected whole round core samples from clast-rich units.

This investigation was initiated with the main aim of refining a preliminary petrographical characterization of the basement clasts within the CRP-2/2A core (Cape Roberts Science Team, 1999), in order to compare their features with those described for similar clasts from the

CRP-1 drillcore (Talarico & Sandroni, 1998), and with those typical of the most likely source rock units within the inland sector of the Transantarctic Mountains facing the drillsite area.

The results further support the previous suggestions of a local provenance for basement clasts, and glacial transport and deposition in the CRP drillsite area.

GEOLOGICAL SETTING, VARIABILITY AND PRELIMINARY PETROGRAPHICAL, SHAPE AND FABRIC CHARACTERISATION OF CRP-2/2A BASEMENT CLASTS

The CRP-2/2A drillhole is located on the western edge of the Victoria Land Basin, at the western margin of the Ross Sea continental shelf (Cooper & Davey, 1987). The onshore region, corresponding to the southern Victoria Land sector of the Transantarctic Mountains, comprises a late Precambrian- Early Paleozoic crystalline basement of granitoids (Granite Harbour Igneous Complex) and metamorphic rocks (Koettlitz Group) (Stump, 1995, and ref. therein). This crystalline basement is overlain by a quartzose sedimentary cover of Devonian to Triassic age (Beacon Supergroup) and intruded by dolerite sills and dykes of Jurassic age (Ferrar Supergroup). Lavas and pyroclastic rocks (Kirkpatrick Basalt) are another significant component of the Ferrar Supergroup in the

region to the west of Cape Roberts, whereas Cenozoic alkalic volcanics of the McMurdo Volcanic Group crop out to the east and south of McMurdo Sound.

The significant and persistent supply of basement-derived pebbles, and the dominance of glacial sedimentary facies throughout most of the recovered sedimentary strata of the western edge of the Victoria Land Basin has already been documented by previous boreholes (CIROS-1, MSSTS, CRP-1) in the McMurdo Sound area. In the Quaternary strata recovered by MSSTS, pebbles of granitoid and metamorphic rocks have been reported (Barrett et al., 1987), and similar contributions were recognized in the Miocene record of the core (Barrett et al., 1986). Basement pebbles including granites, granitic gneisses and biotite schists (George, 1989) were reported as forming a large proportion (35 to 80%) of the clasts in CIROS-1 (Hambrey et al., 1989). Shape characteristics of CIROS-1 clasts indicated subglacial transport with ice grounded or calving at sea level throughout time represented by the core (Hall, 1989). This glacial character was supported by two dimensional fabric analysis (Hambrey et al., 1989). Dominant undeformed or foliated biotite \pm hornblende monzogranites were found in both the Quaternary and lower Miocene sections of the CRP-1 core (Talarico & Sandroni, 1998). Shape and fabric analysis of CRP-1 clasts again suggested subglacial transport with grounded ice or waterlain deposition (Cape Roberts Science Team, 1998b, 1998c).

Results of preliminary investigations on CRP-2/2A basement clasts (Cape Roberts Science Team, 1999) indicated that all the main rock units which underlie the present-day western shore of McMurdo Sound are potential sources for the supply of detritus to the CRP-2/2A site. The CRP-2/2A drillhole recovered a succession consisting of Pliocene-Quaternary (mainly) glacial sediments down to 26.75 metres below the sea floor (mbsf), and, below this, a late Paleogene-early Neogene glacial successions down to 624.15 mbsf (terminal depth).

In the Quaternary-Pliocene section, 689 clasts (granules to boulder grain-size classes) were classified lithologically and counted. In the Quaternary (Lithostratigraphic Unit 2.1: Cape Roberts Science Team, 1999), the number of clasts was found to range between *c.* 50 and 100 *per* metre-length of core, diminishing in abundance near the base of the unit. The main rock types included: granitoids (mainly grey and pink biotite \pm hornblende monzogranites and minor microgranites, showing two peaks at *c.* 11 and 15 mbsf), dolerites (more abundant than granitoids between 17 and 20 mbsf), vesicular basalts (restricted to the *c.* 9-10 mbsf interval) and sedimentary rocks (mainly diamictite, quartzose sandstone, siltstone, characterised by marked fluctuations in abundance and a significant upward increase). In the Pliocene strata (Lithostratigraphical Unit 2.2) the clast population was found to be very similar to that in Unit 2.1 but with a higher content of granitoids and basalt clasts (restricted to *c.* 24-25 mbsf). The similarity between Unit 2.1 and Unit 2.2 is emphasised by clast shape analysis which shows that all samples have broad roundness distributions and significant percentages of faceted clasts, but some samples displaying striated dolerite and sedimentary clasts (Cape Roberts Science Team, 1999).

The granitoids were found to be petrographically similar to those occurring in CRP-1 (Talarico & Sandroni, 1998).

In the Miocene-Oligocene interval, 20 503 clasts, ranging in dimension from granule to boulder grade, were logged and counted on the basis of both approximate grain-size and lithology. This clast population, dominated by granules and fine to coarse pebbles, but also including minor cobbles and rare boulders, consists of seven major lithological groups, namely Cambro-Ordovician granitoids, Ferrar dolerite, McMurdo Volcanic Group alkaline vesicular basalts (Cape Roberts Science Team, 1999), Koettlitz Group Ca-silicate rocks, non vesicular olivine-free basalts (most likely derived from Kirkpatrick Basalt or from chilled margins of Ferrar dolerite sills), McMurdo Volcanic Group pumice (Cape Roberts Science Team, 1999) and sedimentary rocks (including both intraformational and Beacon Supergroup sedimentary rocks). Most lithological boundaries, as well as sequence boundaries, are marked by significant variations in both clast content and in the relative proportions of the main lithologies, and/or the first or last appearance of particular lithologies. In diamict units, the clast content averages 50-100 clasts *per* metre, with values very close to 200 in Lithostratigraphical Unit 12.1. Grain size ranges from granule to boulder (the latter rare and restricted to Units 12.1 and 13.1), with granules and fine to coarse pebbles forming the most represented grain-size classes. In contrast, the sand or mud dominated units are characterised by distinctly lower clast content (usually <10), and grain-size typically ranges from granule (the most abundant) to pebble.

A major change in the distribution pattern of the clast types was recognized to occur at *c.* 310 mbsf, with granitoid-dominated clasts above and mainly dolerite clasts below (Fig. 1). Moreover, a slight increase in grain size within the pebble class and in the number of cobbles was observed moving from the upper to the lower part of the core, particularly below *c.* 300 mbsf. The detailed analysis of compositional and modal data also led to a further division of the Miocene-Oligocene clast population into seven main detrital assemblages or petrofacies (P1 to P7) (Fig. 1). The main compositional features and trends within each petrofacies are revised and summarized here below, taking into account the preliminary description presented in Cape Roberts Science Team (1999).

P1 (26.70 to *c.* 150 mbsf): In this assemblage, granitoid clasts are usually more abundant than dolerite (*c.* 80-60%), but the proportion of dolerite increases slightly with depth. Other rock types are impersistent and much less common. They include: vesicular basalts (six occurrences: at *c.* 36, 77-80, 94, 122, 132 and 140-144 mbsf), pumice (forming the only clast type at 109-114 mbsf, but also occurring as a few scattered clasts at *c.* 101, 116, 122, 132 and 141-143 mbsf), and rare metamorphic rocks mainly consisting of very fine grained, thinly layered Ca-silicate rocks (at *c.* 79, 88, 115, 124 and 142 mbsf). *P1* granitoids consist mainly of grey medium to coarse grained, undeformed or foliated, biotite monzogranite, minor biotite-hornblende granodiorite, and rare biotite-bearing microgranite, grey biotite syenogranite, foliated tonalite and hornblende-bearing monzogranitic porphyry. Shape analysis on four whole round core samples from diamictite units at

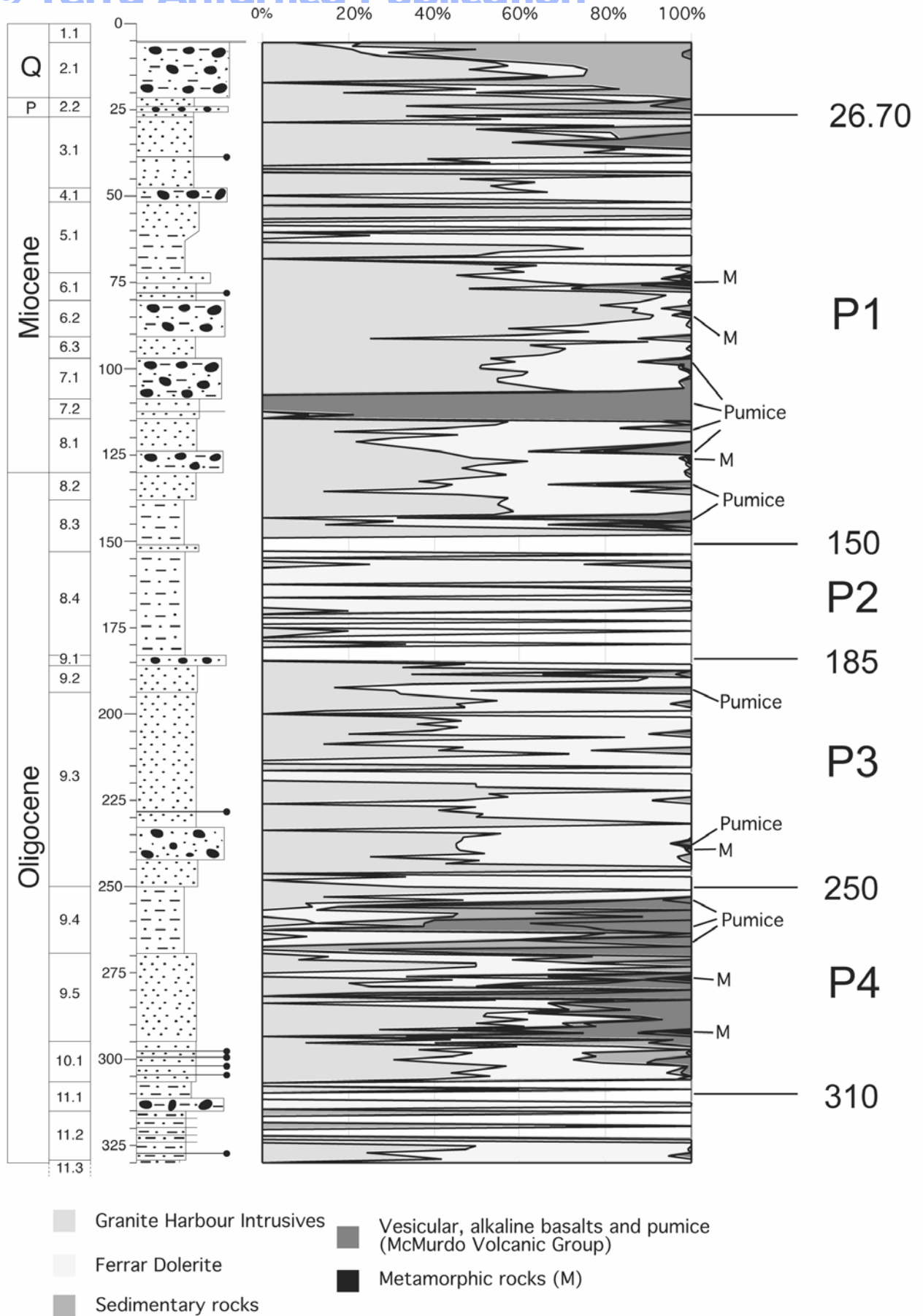


Fig. 1 - Relative proportions of major clast types plotted against depth. Stratigraphical column after Cape Roberts Science Team (1999) (Q = Quaternary, P = Pliocene). P1-P7 = main detrital assemblages or petrofacies.

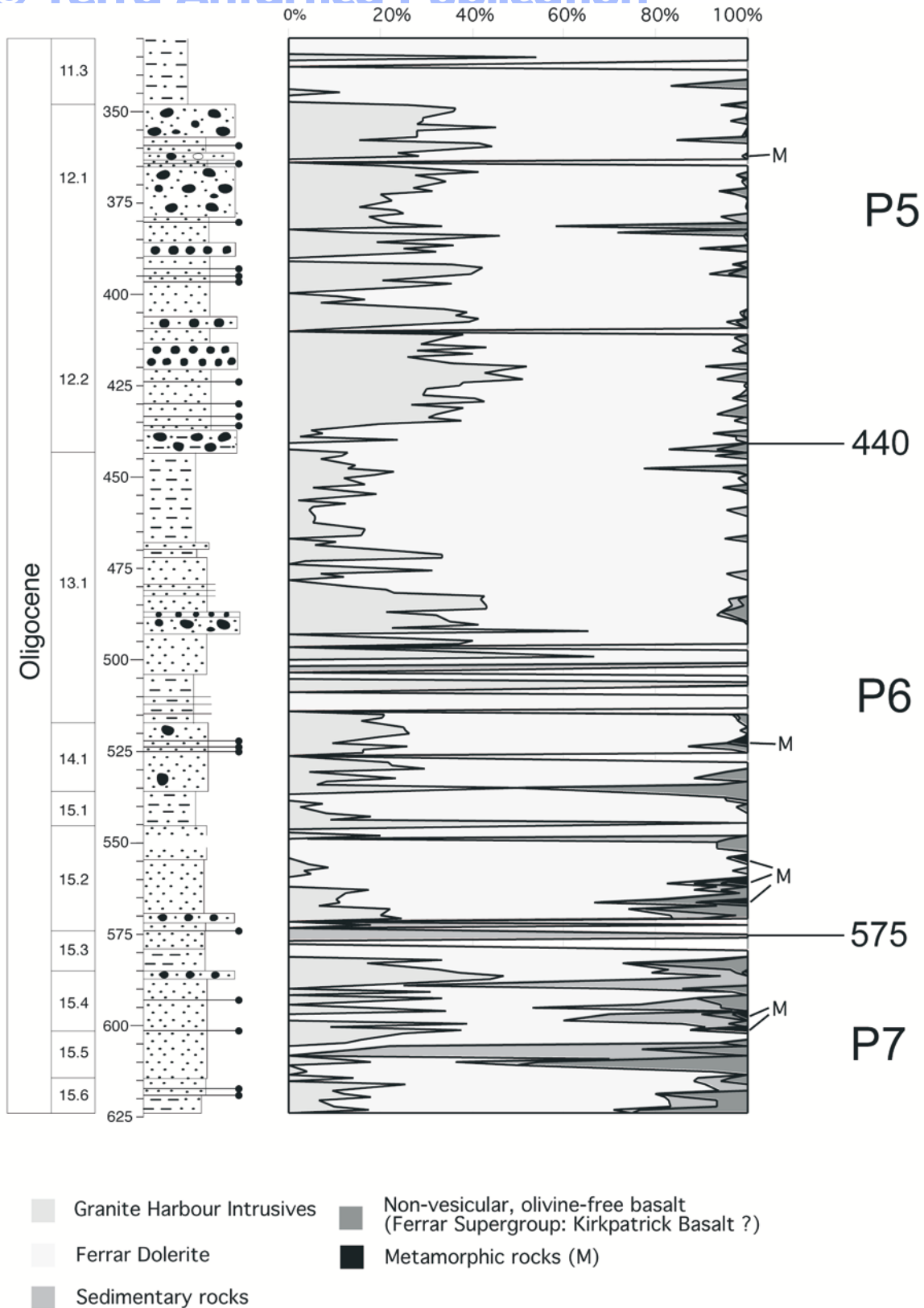


Fig. 1 - Continued.

48.60-48.80, 101.67-101.85, 121.59-121.79 mbsf and a conglomerate at 124.92-125.92 mbsf show broad roundness distributions with a significant percentage (between 23% and 44%) of faceted clasts (*cf.* Fig. 3.9 in Cape Roberts Science Team, 1999). Clast fabric for these samples is weak or random and indicative of waterlain deposits or

post-depositionally deformed grounded ice deposits and the conglomerate suggests a period of short fluvial transport (Cape Roberts Science Team, 1999).

P2 (from c. 150 to c. 185 mbsf): The second petrofacies is characterized by low clast concentrations, with dolerite forming the dominant lithology, and a very low proportion

of granitoids, mainly consisting of grey and pink biotite monzogranites. The only additional rock type present consists of a few clasts of intraformational sedimentary rocks (quartz-rich sandstone, black volcanoclastic siltstone).

P3 (from *c.* 185 to *c.* 250 mbsf): The third assemblage shows subequal proportions of dolerite and granitoids (mainly pink biotite±hornblende monzogranite), but it also includes minor vesicular basalt (at *c.* 178, 194, 198 mbsf), rare Ca-silicate rock (at *c.* 238 mbsf) and pumice clasts (at *c.* 194 mbsf). A whole round core sample near the base of this zone at 233.80-234.04 mbsf again displays broad roundness and a high number of faceted and weak fabric (*cf.* Figs. 3.7 and 3.9, Cape Roberts Science Team, 1999).

P4 (from *c.* 250 to *c.* 310 mbsf): This assemblage shows a slight increase downcore in granitoid clasts and a decrease in dolerite. *P4* granitoids are mainly pink monzogranite, minor grey monzogranite and rare pink granitic and monzonitic porphyries. Vesicular basalt and sedimentary rocks are also major components. They are persistent but abundances fluctuate sharply. The sedimentary rocks are mainly intraformational clasts of grey and black siltstone, but they also include a few possible Beacon Supergroup sedimentary rocks (well consolidated black siltstone with calcite veins at *c.* 292 mbsf and quartz arenite at *c.* 293 mbsf).

P5 (from *c.* 310 to *c.* 440 mbsf): The clast assemblage in *P5* is broadly similar to *P3* but contains dissimilar scarce and impersistent volcanic clasts of non vesicular basalts (?Kirkpatrick Basalts) and rare clasts of gneiss and Ca-silicate (at *c.* 360 and *c.* 385 mbsf). Clasts of intraformational black siltstone or sandstone are also present. Granitoid pebbles in *P5* consist mainly of pink or grey, foliated or undeformed, biotite monzogranite, but pink-orange microgranite and monzogranitic porphyry are also widespread and abundant, particularly below 362 mbsf. Minor lithologies include biotite±hornblende granodiorite and quartz monzogabbro. Three sandy diamictites at 351.37-351.67, 372.15-372.46, 406.80-407.09 mbsf and one conglomerate at 387.02-387.32 mbsf whole round core samples from this zone shows broad roundness distributions and significant faceting. All except sample 372.15-372.46 mbsf contained a few striated dolerite and sedimentary clasts. A weak preferred clast orientation occurs in sample 351.32-351.67 mbsf and the other samples are show random fabric. (Figs. 3.7 & 3.9, Cape Roberts Science Team, 1999). A strong glacial influence is again inferred but also includes limited fluvial transport for sample 387.02-387.32 mbsf.

P6 (from *c.* 440 to *c.* 575 mbsf): This petrofacies shows a broad peak in granitoid clast abundances at *c.* 475-500 mbsf, and a highly variable content of non vesicular basalts (mainly concentrated at *c.* 530-540 and 560-570 mbsf). Rare clasts of Ca-silicate rock and gneiss occur at *c.* 524, 559, 565 and 570 mbsf. Sedimentary clasts include intraformational siltstone, minor Beacon Supergroup(?) quartz arenite (at *c.* 562, 566, 573 mbsf), and dispersed coal (mainly occurring below *c.* 486 mbsf). *P6* granitoid clasts are mainly grey to pink-grey biotite monzogranite and minor biotite-hornblende±clinopyroxene granodiorite.

Pink-orange monzogranitic porphyry is also common throughout *P6*. The three deepest whole round samples are within this zone and are dominated by dolerite. Roundness distribution is broad with up to 50 percent of clasts faceted (sample 518.32-518.62 mbsf) but without any striated clasts. A sample at 441.22-441.52 mbsf displays random fabric and samples at 490.10-490.39 and 518.32-518.62 mbsf have only weak preferred orientation.

P7 (from *c.* 575 to 625 mbsf): This assemblage shows significant fluctuations in the proportions of granitoids (mainly grey and pink biotite±hornblende monzogranites, minor biotite granodiorite and orange monzogranitic porphyry) and dolerite clasts, but the granitoids generally decrease downcore antipathetic to the proportions of non vesicular basalts. There are a few sedimentary clasts (mainly coal and Beacon Supergroup(?) quartz arenite) and a few metamorphic clasts (a biotite orthogneiss at *c.* 588 mbsf, and a biotite-clinzoisite schist at *c.* 599 mbsf).

PETROGRAPHICAL FEATURES, GEOCHEMISTRY AND MINERAL CHEMISTRY

PETROGRAPHY

The main petrographical characteristics of the most common lithologies which form the pebble- to cobble-grain size fraction in the Quaternary-Pliocene and Lower Miocene-Oligocene sections of the CRP-2/2A core are here reported with particular focus on the dominant plutonic and subordinate metamorphic rock types. Representative samples to show the lithological range and the mineral assemblages typical of most common basement clasts throughout the borehole are listed in table 1.

Like CRP-1 basement clasts, most samples show a variably developed, but commonly extensive alteration which affected the primary mineral assemblages through static, strain-free transformations (pseudomorphs and reaction rims) under low temperature, greenschist to subgreenschist facies conditions. These mineral transformations include the partial to complete replacement of calcic plagioclase by saussurite (sericite-albite±epidote±calcite), the replacement of K-feldspar by sericite or kaolinite microaggregates (commonly more advanced in pink or red-coloured granitoids and porphyries than in the grey varieties), the partial transformation of Mg-hornblende into actinolite and/or chlorite, and the extensive alteration of red-brown biotite into Fe-Mg or Mg-Fe chlorite and/or prehnite+titanite±opaque minerals.

In the Pliocene-Quaternary interval, granitoid pebbles are mainly grey or pink biotite±hornblende monzogranites and minor pink-grey biotite-bearing microgranites.

In the Miocene-Oligocene strata, a more varied lithological range occurs. Grey or pink, biotite±hornblende monzogranites, mostly undeformed but with rare foliated varieties, still represent the dominant lithology, but other rock types, although much less common, are present: biotite-hornblende±clinopyroxene granodiorite, grey biotite syenogranite, foliated clinopyroxene-bearing tonalite, biotite-bearing haplogranite, biotite±hornblende-

Tab. 1 - Petrographical classification and mineral assemblages of representative samples of basement clasts from the Quaternary-Pliocene and Miocene-Oligocene sections of the CRP-2/2A borehole.

Sample code	Top (mbsf)	Clast shape	Approximate size (cm)	Lithology	Mineral assemblage	Lithostratigraphic Unit
CRP2-TAL1	5.70	subrounded	20x6x3	Pink-grey biotite-bearing microgranite	Kfs (34%), Qtz (32%), Pl (30%), Bt (3%), Ms (s), Chl (s), Ttn (s), Opm (t), Ap (t), Zrn/Mnz (t)	2.1
CRP2-TAL2	12.21	subrounded	5x3x3	Pink-grey biotite-bearing microgranite	Qtz (36%), Kfs (32%), Pl (30%), Bt (1%), Ms (s), Opm (t), Ap (t), Zrn/Mnz (t)	2.1
CRP2-TAL3	15.32	subangular	40x6x3	Grey biotite monzogranite	Pl (33%), Kfs (32%), Qtz (30%), Bt (5%), Opm (t), Ap (t), Chl (s), Ttn (s), Ms (s)	2.1
CRP2-TAL4	19.46	subrounded	8x4x3	Pink biotite-hornblende monzogranite	Kfs (38%), Qtz (30%), Pl (25%), Hbl (4%), Bt (3%), Czo-Ep (s), Ms (s), Chl (s), Aln (t), Opm (t), Ap (t), Zrn/Mnz (t)	2.1
CRP2-TAL5	39.16	subrounded	12x6x3	Grey biotite-bearing monzogranite	Pl (34%), Kfs (33%), Qtz (32%), Bt (1%), Opm (t), Ap (t), Chl (s), Ttn (s), Ms (s), Zrn/Mnz (t)	3.1
CRP2-TAL6	48.17	subangular	4x2x2	Hornblende-bearing monzogranitic porphyry	Pl (42%), Kfs (30%), Qtz (25%), green Hbl (3%), Ms (s), Chl (s), Czo-Ep (s), Opm (t), Zrn (t), Ap (t)	4.1
CRP2-TAL7	49.39	subrounded	12x6x3	Biotite-hornblende granodiorite	Pl (44%), Qtz (29%), Kfs (12%), green Hbl (8%), Bt (7%), Ms (s), Chl (s), Aln (t), Ap (t), Zrn/Mnz (t)	4.1
CRP2A-TAL9	73.30	subrounded	12x3x3	Grey biotite-bearing monzogranite	Pl (35%), Kfs (32%), Qtz (32%), Bt (1%), Opm (t), Ap (t), Aln (t), Chl (s), Ttn (s), Ms (s)	6.1
CRP2A-TAL11	79.51	rounded	4x2x2	Biotite-bearing monzogranitic porphyry	Pl (40%), Kfs (32%), Qtz (24%), Bt (4%), Ms (s), Chl (s), Opm (t), Zrn (t), Ap (t)	6.1
CRP2A-TAL12	81.93	subangular	6x2x3	Grey biotite monzogranite	Qtz (37%), Pl (31%), Kfs (29%), Bt (3%), Ms (s), Chl (s), Opm (t), Aln (t), Zrn (t)	6.2
CRP2A-TAL13	87.97	subrounded	2.5x2x3	Grey foliated biotite monzogranite	Pl (33%), Kfs (32%), Qtz (32%), Bt (3%), Ms (s), Chl (s), Opm (t), Ap (t), Zrn/Mnz (t)	6.2
CRP2A-TAL14	88.23	subangular	3x2x1.5	Ca-silicate rock	Pl (40%), Cpx (30%), Qtz (17%), Bt (13%), Act-Hbl (s), Kfs (t), Ms (s), Chl (s), Ttn (t), Opm (t), Zrn/Mnz (t)	6.2
CRP2A-TAL15	97.68	subrounded	5x4x3	Grey biotite monzogranite	Qtz (35%), Pl (32%), Kfs (31%), Bt (2%), Ms (s), Chl (s), Opm (t), Zrn (t)	7.1
CRP2A-TAL20	106.41	subangular	11x6x3	Ca-silicate rock	Cpx (40%), Kfs (25%), Pl (22%), Bt (13%), Ms (s), Chl (s), Ttn (t), Opm (t), Zrn/Mnz (t)	7.1
CRP2A-TAL22	122.00	subrounded	7x6x3	Grey garnet-bearing biotite monzogranite	Qtz (38%), Pl (27%), Kfs (24%), Grt (1%), Ms (s), Chl (s), Opm (t)	8.1
CRP2A-TAL23	124.62	subangular	3x2x1.5	Greyish-pink biotite-bearing haplogranite	Qtz (35%), Pl (32%), Kfs (31%), Bt (2%), Ms (s), Chl (s), Opm (t), Zrn/Mnz (t)	8.1
CRP2A-TAL24	127.44	subrounded	5x4x4	Grey biotite syenogranite	Kfs (43%), Qtz (35%), Pl (17%), Bt (5%), Opm (t), Aln (t), Ms (s), Zrn/Mnz (t)	8.1
CRP2A-TAL25	128.58	subangular	5.5x4x3	Foliated clinopyroxene-bearing tonalite	Pl (45%), Bt (18%), Qtz (15%), Cpx (12%), Hbl (10%), Opm, Chl (s)	8.1
CRP2A-TAL26	238.68	angular	4x1.5x1.5	Ca-silicate rock	Cpx (40%), Pl (25%), Cal (18%), Qtz (17%), green Act-Hbl (s), Czo-Ep (s), Ms (s), Chl (s), Ttn (t), Opm (t), Zrn/Mnz (t)	9.3
CRP2A-TAL27	240.70	subrounded	8x4x4	Pink hornblende-biotite monzogranite	Kfs (36%), Qtz (31%), Pl (26%), Hbl (4%), Bt (3%), Ms (s), Chl (s), Aln (t), Opm (t), Ap (t), Zrn/Mnz (t)	9.3
CRP2A-TAL30	293	subrounded	1.5x.2x1	Greenish monzonitic porphyry	Pl (49%), Kfs (46%), Qtz (5%), Ms (s), Chl (s), Czo-Ep (s), Opm (t), Zrn (t), Ap (t)	9.5

Tab. 1 - Continued.

Sample code	Top (mbsf)	Clast shape	Approximate size (cm)	Lithology	Mineral assemblage	Lithostratigraphic Unit
CRP2A-TAL33	348.81	subrounded	1.5x2x1	Pink biotite monzogranite	Qtz (42%), Kfs (30%), Pl (27%), Bt (1%), Opm (t), Ms (s), Chl (s), Ttn (s), Zrn/Mnz (t)	12.1
CRP2A-TAL34	349.39	subrounded	57x4.5x2.7	Grey foliated biotite monzogranite	Pl (34%), Kfs (32%), Qtz (30%), Bt (4%), Ms (s), Chl (s), Opm (t), Aln (t), Ap (t), Zrn/Mnz (t)	12.1
CRP2A-TAL36	367.70	subrounded	12x2.5x2	Grey foliated biotite monzogranite	Kfs (34%), Qtz (32%), Pl (28%), Bt (6%), Ms (s), Chl (s), Opm (t), Zrn/Mnz (t)	12.1
CRP2A-TAL40	375.58	subrounded	4.5x5x2.5	Pink-orange biotite-hornblende monzogranitic porphyry	Pl (35%), Kfs (39%), Hbl (5%), Bt (4%), Qtz (22%), Ms (s), Chl (s), Czo-Ep (s), Opm (t), Zrn (t), Ap (t)	12.1
CRP2A-TAL41	378.98	rounded	4.5x4x2.5	Biotite-hornblende granodiorite	Pl (42%), Qtz (31%), Kfs (10%), green Hbl (9%), Bt (8%), Ms (s), Chl (s), Aln (t), Ap (t), Zrn/Mnz (t)	12.1
CRP2A-TAL42	385.18	subrounded	1.5x1x2	Biotite granodiorite	Pl (50%), Qtz (25%), Kfs (18%), Bt (7%), Ms (s), Chl (s), Opm (t), Aln (t), Ap (t), Zrn/Mnz (t)	12.2
CRP2A-TAL43	385.83	subrounded	4x5x2.5	Biotite-hornblende quartz monzogabbro	Pl (45%), Kfs (13%), green Hbl (20%), Bt (15%), Qtz (7%), Ms (s), Chl (s), Ap (t), Ttn (t), Opm (t), Zrn/Mnz (t)	12.2
CRP2A-TAL44	388.62	subrounded	7x4.5x2.5	Pink-orange biotite-bearing monzogranitic porphyry	Pl (38%), Kfs (33%), Qtz (26%), Bt (3%), Ms (s), Chl (s), Opm (t), Zrn (t), Ap (t)	12.2
CRP2A-TAL45	407.70	subangular	6x4x2	Grey biotite-hornblende monzogranite	Kfs (31%), Qtz (29%), Pl (33%), Hbl (4%), Bt (3%), Ms (s), Chl (s), Aln (t), Opm (t), Ttn (t), Ap (t), Zrn/Mnz (t)	12.3
CRP2A-TAL46	487.57	subrounded	4x3x2	Clinopyroxene-biotite-hornblende granodiorite	Pl (44%), Qtz (24%), Kfs (12%), Cpx (9%), green Hbl (7%), Bt (4%), Ms (s), Chl (s), Ap (t), Zrn/Mnz (t)	13.2
CRP2A-TAL47	488.82	subangular	2x1.5x3	Pink-grey biotite-bearing monzogranite	Pl (31%), Kfs (31%), Qtz (30%), Bt (8%), Ms (s), Chl (s), Opm (t), Aln (t), Ap (t), Zrn/Mnz (t)	13.2
CRP2A-TAL49	489.6	rounded	5x4x2	Pink biotite monzogranite	Kfs (34%), Pl (32%), Qtz (29%), Bt (5%), Ms (s), Chl (s), Opm (t), Aln (t), Ap (t), Zrn/Mnz (t)	13.2
CRP2A-TAL50	519.11	subrounded	11x4x2.5	Pink-grey biotite monzogranite	Pl (35%), Kfs (31%), Qtz (30%), Bt (4%), Ms (s), Chl (s), Opm (t), Aln (t), Ap (t), Zrn/Mnz (t)	14.1
CRP2A-TAL51	569.64	rounded	8x4.5x2.5	Hornblende-biotite granodiorite	Pl (46%), Qtz (28%), Kfs (11%), green Hbl (9%), Bt (8%), Ms (s), Chl (s), Ap (t), Zrn/Mnz (t)	15.2
CRP2A-TAL52	569.83	rounded	2x2x1.5	Biotite-bearing monzogranitic porphyry	Pl (39%), Kfs (32%), Qtz (25%), Bt (4%), Ms (s), Chl (s), Opm (t), Zrn (t), Ap (t)	15.2
CRP2A-TAL57	587.94	subangular	3x2x1	Biotite orthogneiss	Pl (35%), Qtz (33%), Bt (17%), Kfs (15%), Ms (s), Opm (t), Ap (t), Zrn (t)	15.4
CRP2A-TAL61	592.82	rounded	2x1x1	Pink biotite monzogranite	Pl (33%), Kfs (32%), Qtz (30%), Bt (5%), Ms (s), Chl (s), Opm (t), Aln (t), Ap (t), Zrn/Mnz (t)	15.4
CRP2A-TAL62	596.83	rounded	1.5x1.5x1	Orange monzogranitic porphyry	Pl (40%), Kfs (31%), Qtz (27%), Bt (2%), Ms (s), Chl (s), Opm (t), Zrn (t), Ap (t)	15.4
CRP2A-TAL63	599.28	angular	3x1.5x1.5	Biotite-clinozoisite schist	Bt (28%), Czo/Ep (21%), Qtz (20%), Pl (18%), Ms (13%), Opm (t), Zrn (t)	15.4
CRP2A-TAL64	600.77	rounded	32x4x2.5	Grey hornblende-biotite monzogranite	Kfs (33%), Qtz (31%), Pl (26%), Bt (6%), Hbl (4%), Ms (s), Chl (s), Aln (t), Opm (t), Ap (t), Zrn/Mnz (t)	15.5
CRP2A-TAL65	614.24	rounded	9x4.5x2.5	Pink-grey biotite granodiorite	Pl (45%), Qtz (35%), Kfs (16%), Bt (4%), Ms (s), Chl (s), Opm (t), Aln (t), Ap (t), Zrn/Mnz (t)	15.6

Note: mineral abbreviations are according to Kretz (1983) (with the addition of Opm to indicate opaque minerals). Modal contents of essential phases are given as percentages. t = trace (<1% modal content), s = mineral phase of secondary origin. Lithostratigraphic unit designation from Cape Roberts Science Team (1999).

bearing monzogranitic to monzonitic porphyries, quartz monzogabbro, Ca-silicate rock and biotite gneiss (Tab. 1).

Grey and pink biotite±hornblende monzogranites (15.32, 19.46, 39.16, 73.30, 81.93, 97.68, 240.70, 348.81, 407.70, 488.82, 489.60, 519.11, 592.82, 600.77 mbsf) are fine- to medium/coarse-grained and their textures are commonly equigranular to heterogranular and hypidiomorphic to allotriomorphic. Alkali feldspar is micropertitic orthoclase or microcline, often occurring as anhedral phenocrysts transformed into a felty micro-aggregate of kaolinite or sericite. Plagioclase (oligoclase-andesine) forms subhedral to euhedral laths which commonly show a marked normal compositional zoning and are partly transformed into sericite or saussurite. Red-brown biotite is in places intergrown with euhedral crystals of green hornblende and it is partly replaced by FeMg-chlorite±prehnite±epidote. Rare garnet, forming small subhedral grains, was found only in one sample (122.00 mbsf). Typical accessory phases (Tab. 1) include opaque minerals (commonly ilmenite), apatite, monazite/zircon and allanite. Grey foliated biotite monzogranite (87.97, 349.39, 367.70 mbsf) are characterized by similar mineral assemblages but their fabrics show a number of features, such as sub-grains boundaries, wave extinction, kink-bands, deformation twins and a weak to marked foliation defined by recrystallized feldspars and biotite, which are all indicative of solid-state deformation.

Biotite-hornblende granodiorites (49.39, 378.98, 385.18, 569.64, 614.24 mbsf) are heterogranular, fine- to medium-grained and hypidiomorphic. Both plagioclase (normally zoned: an40-32) and K-feldspar (micropertitic orthoclase) occur as subhedral laths carrying fine grained inclusions of biotite and quartz. Biotite and hornblende define a weak foliation. Quartz occurs as interlobate granular aggregates, as well as highly strained grains mantled by sub-polygonal aggregates of finer-new grains. Clinopyroxene-bearing varieties (487.57 mbsf) are characterized by similar petrographical features, except for the occurrence of skeletal relics of clinopyroxene within green hornblende.

Foliated clinopyroxene-bearing tonalite (128.58 mbsf) is characterized by a marked foliation defined by parallel alignment of plagioclase (an35) laths, of quartz polycrystalline aggregates, and of red-brown biotite flakes. Both plagioclase and biotite show prominent kink-bands and primary quartz crystals are almost completely replaced by sub-polygonal aggregates. Clinopyroxene is present as anhedral crystals, partly replaced by green hornblende±chlorite, and accessory phases include titanite, allanite and opaque minerals.

Biotite-hornblende quartz monzogabbro (385.83 mbsf) is heterogranular, fine to medium-grained and hypidiomorphic-subophitic; plagioclase is present as subhedral laths showing normal zoning and labradorite (an66) cores; both micropertitic K-feldspar and quartz occur as poikilitic crystals carrying inclusions of plagioclase, green hornblende (replaced by actinolite±chlorite) and biotite (transformed to chlorite±titanite). Accessory phases include opaque minerals, titanite, apatite and zircon/monazite.

Pink-grey biotite-bearing microgranites (5.70, 12.21, 124.62 mbsf) are very fine- to fine-grained, with interlobate to sub-polygonal granular textures and low modal contents of red-brown biotite. In these rocks K-feldspar typically occurs as poikilitic crystals carrying rounded inclusions of oligoclase, quartz and brown biotite partly replaced by Fe-Mg chlorite±prehnite.

Biotite±hornblende-bearing monzogranitic porphyry (48.17, 79.51, 375.58, 388.62, 569.83, 596.83 mbsf) consists of idiomorphic phenocrysts of orthoclase/microcline (micropertitic and replaced by clay mineral microaggregates or sericite), sericitized oligoclase, and quartz set within a very fine to fine-grained felsic groundmass consisting of plagioclase, quartz and

K-feldspar with scattered aggregates of red-brown biotite, green hornblende, opaque minerals, titanite and white mica.

Ca-silicate rocks (88.23, 106.41, 238.68 mbsf) are characterised by fine grain-sizes and interlobate to subpolygonal granonematoblastic textures, with a marked foliation defined by the preferential dimensional orientation of clinopyroxene and biotite. Millimetre-scale compositional layerings are composed by granoblastic layers of plagioclase, quartz and clinopyroxene, alternating with granolepidoblastic layers consisting of plagioclase, quartz, clinopyroxene and biotite (or K-feldspar)±green hornblende/actinolite. Accessory minerals include abundant titanite (up to 3%), ilmenite and zircon/monazite.

Biotite-clinozoisite schist (599.28 mbsf) is fine-grained with a marked foliation defined by clinozoisite and biotite. The mineral assemblage also includes quartz and plagioclase (an15) forming interlobate granoblastic aggregates, muscovite, and accessory opaque minerals and zircon.

Biotite orthogneiss (587.94 mbsf) shows a simple mineral assemblage of plagioclase (an35), quartz, biotite, K-feldspar, muscovite (secondary phase after feldspars), opaque minerals, apatite and zircon. This rock shows a marked foliation defined by biotite and muscovite lamellae which wrap around strained porphyroclasts of plagioclase and K-feldspar.

GEOCHEMISTRY

A few clasts were found with appropriate features, such as size and low degree of low temperature alteration, to allow whole-rock geochemical analyses. Nine selected samples of granitoids, including one sample from the Pliocene-Quaternary section, have been analyzed for major and trace elements by XRF following the procedures of Franzini et al. (1975) and Leoni & Saitta (1976). FeO was determined by titration, MgO and Na₂O by Atomic Absorption Spectrometry, and loss on ignition by gravimetry at 960 °C, after preheating at 110 °C.

The analytical data are listed in table 2. Analyzed granitoids include three undeformed biotite monzogranites (CRP2-TAL3, CRP2A-TAL9, CRP2A-TAL49), two foliated biotite monzogranites (CRP2A-TAL34, CRP2A-TAL36), one mesocratic biotite-hornblende monzogranite (CRP2A-TAL64), one biotite granodiorite (CRP2A-TAL65) and two monzogranitic porphyries (CRP2A-

Tab. 2 - Selected major elements (wt%) and trace elements (ppm) and C.I.P.W. norms of CRP-2/2A basement clasts.

	CRP2A TAL64	CRP2A TAL44	CRP2A TAL40	CRP2A TAL65	CRP2A TAL9	CRP2A TAL34	CRP2A TAL36	CRP2 TAL3	CRP2A TAL49
SiO ₂	63.38	70.71	70.98	71.42	72.44	72.81	73.33	73.52	73.96
TiO ₂	0.92	0.29	0.30	0.44	0.29	0.23	0.19	0.22	0.17
Al ₂ O ₃	15.34	13.93	14.18	13.60	13.51	14.39	14.43	13.10	13.67
Fe ₂ O ₃	1.17	0.28	0.33	1.63	0.58	0.27	0.65	0.63	0.25
FeO	4.26	1.85	2.37	1.39	1.27	1.32	0.49	1.20	1.18
MnO	0.09	0.04	0.06	0.06	0.02	0.04	0.02	0.04	0.03
MgO	2.28	0.52	0.46	1.15	0.48	0.44	0.61	0.36	0.39
CaO	4.54	1.81	1.64	3.20	1.41	2.15	2.68	1.41	1.79
Na ₂ O	3.24	3.08	3.72	3.86	3.10	3.84	3.38	3.02	3.51
K ₂ O	3.23	5.03	5.08	0.82	5.98	3.81	3.25	5.48	4.03
P ₂ O ₅	0.27	0.08	0.05	0.12	0.05	0.05	0.04	0.03	0.04
L.O.I.	1.27	2.38	0.82	2.31	0.85	0.66	0.93	0.98	0.98
total	99.99	100.00	99.99	100.00	99.98	100.01	100.00	99.99	100.00
Nb	18	14	15	9	15	15	6	12	9
Zr	192	207	362	180	205	137	146	184	117
Y	24	21	28	10	22	15	13	14	11
Sr	598	223	298	508	306	505	599	328	391
Rb	98	168	157	30	224	148	92	171	147
Ni	8	1	0	7	0	2	1	1	0
Cr	23	8	4	12	2	6	4	1	4
V	59	14	10	21	11	8	8	7	8
Ba	1105	939	1791	446	894	1181	1345	1154	623
La	33	44	57	28	68	24	23	34	22
Ce	62	81	90	48	109	38	31	47	36
A.S.I.	0.90	1.01	0.97	1.04	0.95	1.00	1.03	0.97	1.02
C.I.P.W. Norms									
Qtz	17.95	27.86	24.34	37.33	27.59	29.91	34.66	31.05	33.03
Or	19.09	29.72	30.02	4.85	35.34	22.51	19.20	32.38	23.81
Ab	27.41	26.06	31.48	32.66	26.23	32.49	28.60	25.55	29.70
An	17.77	8.46	6.99	15.09	5.29	10.34	13.03	6.00	8.62
C	0.00	0.32	0.00	0.83	0.00	0.16	0.58	0.00	0.38
Di	2.47	0.00	0.70	0.00	1.15	0.00	0.00	0.67	0.00
Hy	9.96	4.06	4.48	3.45	2.03	2.99	1.61	1.95	2.71
Ol	0.00	0.00	0.00	0.00	0.00	0.00	0.00	0.00	0.00
Mgt	1.70	0.41	0.48	2.36	0.84	0.39	0.94	0.91	0.36
Rt	0.00	0.00	0.00	0.00	0.00	0.00	0.00	0.00	0.00
Ilm	1.75	0.55	0.57	0.84	0.55	0.44	0.36	0.42	0.32
Ap	0.64	0.19	0.12	0.28	0.12	0.12	0.09	0.07	0.09

TAL40, CRP2A-TAL44). Harker-type variation diagrams and an ASI ($\text{Al}_2\text{O}_3/(\text{K}_2\text{O}+\text{Na}_2\text{O}+\text{CaO})$ molecular ratio) *versus* SiO₂ plot are shown in figure 2. Except for the mesocratic monzogranite CRP2A-TAL64 which shows a distinctly lower silica content and higher FeO, MgO and CaO contents, all other samples plot within a narrow range of SiO₂ (70.71-73.96 wt%), with low MgO (0.36-1.15 wt%), CaO (3.20-1.41 wt%) and FeO (0.49-2.37 wt%) values. All samples show a metaluminous character, as evidenced by normative quartz and hypersthene, with less than 1% normative corundum and A.S.I. values between 0.90 and 1.04.

Overall, the nine analyzed samples are geochemically typical of Granite Harbour Igneous Complex from the Transantarctic Mountains in Victoria Land (Ghezzi et al., 1987; Smillie, 1992; Allibone et al., 1993b). All samples with only one exception plot within or close to the reference compositional fields of the two granitoid suites, DV1 and DV2, as defined by Smillie (1992) and by Allibone et al. (1993b) for the granitoids from South Victoria Land (Fig. 3).

MINERAL CHEMISTRY

Five samples were selected for mineral analysis: undeformed biotite-hornblende monzogranite CRP2A-TAL45, foliated monzogranite CRP2A-TAL34, biotite granodiorite CRP2A-TAL 42, biotite-hornblende quartz monzogabbro CRP2A-TAL43 and Ca-silicate rock CRP2A-TAL14 (Tab. 1).

Chemical analysis of the main mineral phases were carried out with an X-ray energy dispersive system EDAX DX4 attached to a Scansion Electron Microscope Philips XL30, at 20 Kv, 60 mA of emission current and beam spot size of 0.2 mm, using natural minerals as standards. Fe₂O₃ in clin amphiboles and clinopyroxenes was calculated assuming charge balance and the equation given by Papike et al. (1974).

Biotite - Representative compositions are listed in table 3. No significant intra-crystalline compositional zoning was detected. In the undeformed monzogranite (TAL45), biotite composition is characterised by Al^{IV} from 2.46 to 2.56

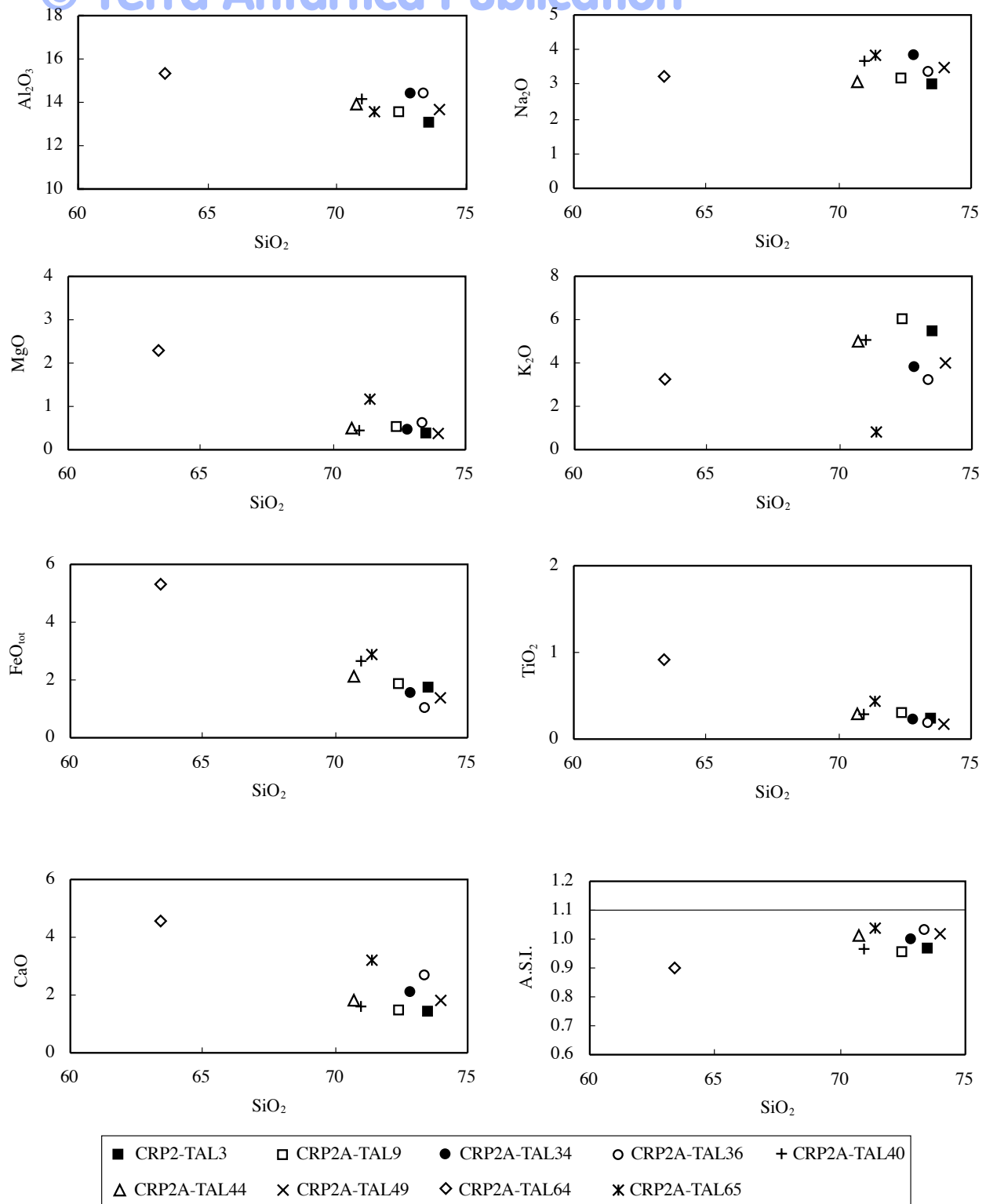


Fig. 2 - Harker-type variation diagrams (all major elements and SiO_2 as wt%) and an ASI ($\text{Al}_2\text{O}_3/(\text{K}_2\text{O}+\text{Na}_2\text{O}+\text{CaO}$ molecular ratio) versus SiO_2 (wt%) plot for CRP-2/2A basement clasts.

(atoms per formula unit, a.p.f.u. on the base of 22 oxygens) and X_{Fe} between 0.65 and 0.60. In the biotite granodiorite (TAL 42), biotite shows similar compositions with Al^{IV} in the range 2.39-2.46 and $X_{\text{Fe}}=0.61-0.63$. In contrast, the foliated monzogranite (TAL34) is characterised by biotite with higher X_{Fe} (Fig. 4); biotite grains occurring as inclusions within K-feldspar or plagioclase phenocrysts

commonly show the highest X_{Fe} values (e.g. 4-i in Tab. 3). No significant compositional differences were detected between recrystallized grains and primary crystals (Tab. 3). Biotite from the quartz monzogabbro (TAL43) has the lowest X_{Fe} values (0.55-0.56). In the $\text{FeO}_{\text{tot}}-\text{MgO}-\text{Al}_2\text{O}_3$ diagram (Rossi & Chevremont, 1987) (Fig. 5), most sample data fall in the calc-alkaline field with the exception

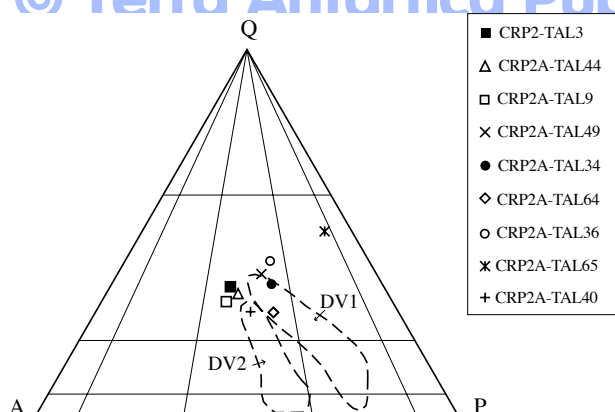


Fig. 3 - Normative QAP compositions of analyses of CRP-2/2A basement clasts (sample symbols as in Fig. 2). Compositions of the DV1 and DV2 plutonic suites of southern Victoria Land, from Smillie (1992), are plotted for comparison.

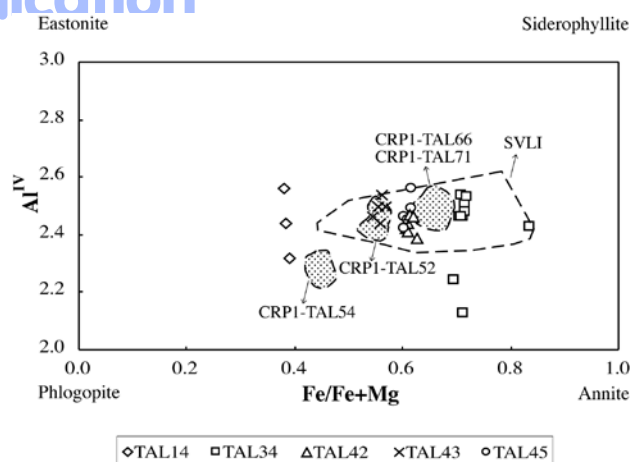


Fig. 4 - Biotite composition in terms of Al^{IV} vs Fe/(Fe+Mg) for CRP-2/2A basement clasts. Contoured field is that of biotite compositions from the calcalkaline South Victoria Land Intrusives (Armienti et al., 1990) on the basis of data reported in Biagini et al. (1991). Compositional fields of biotite from CRP-1 basement clasts (Talarico & Sandroni, 1998) are also shown for comparison (CRP1-TAL66: grey biotite monzogranite, 30.62 mbsf; CRP1-TAL71: foliated biotite monzogranite, 40.90 mbsf; CRP1-TAL52: biotite-hornblende granodiorite, 134.71 mbsf; CRP1-TAL54: Ca-silicate rock, 135.33 mbsf).

of sample TAL45, whose biotite data plot in the Fe-potassic monzonitic field. Biotite from the Ca-silicate rock shows very limited compositional variations: X_{Fe}=0.49-0.48, Al^{IV}=2.32-2.44.

Clinoamphibole and Clinopyroxene - Representative analyses are listed in table 4. In all samples, amphiboles are members of the calcic-amphibole group (Leake, 1978) (Fig. 6). Amphibole from the undeformed biotite-hornblende monzogranite (CRP2A-TAL45) is Fe-hornblende and shows a slight compositional zoning with

Tab. 3 - Representative chemical analyses of biotite in CRP-2/2A basement clasts.

Oxide (wt%)	CRP2A-TAL14		CRP2A-TAL34					CRP2A-TAL42				CRP2A-TAL43		CRP2A-TAL45			
	1	2	1	2	3	4-iPl	5-i/Kfs	6-n	7-n	1	2	3	4	1	2	1	2
SiO ₂	38.44	37.73	35.10	38.52	37.79	35.62	35.66	35.18	35.76	36.63	36.66	36.12	36.48	35.76	36.45	35.94	34.67
Al ₂ O ₃	14.34	14.69	16.39	15.53	16.00	18.89	16.26	16.50	16.27	16.24	15.99	15.84	15.97	14.66	14.61	14.06	13.52
TiO ₂	1.79	1.96	3.69	3.27	3.11	0.57	3.58	4.00	3.75	3.49	3.70	3.69	2.97	5.62	4.80	4.45	5.00
MgO	15.73	16.69	5.84	5.55	5.71	3.02	5.64	5.54	5.79	8.18	7.61	7.92	8.28	9.42	9.99	8.74	7.70
FeO	17.86	18.61	25.39	24.40	23.06	27.77	25.14	24.17	25.12	22.33	22.84	22.96	23.02	21.67	21.41	23.57	25.58
MnO	0.04	0.00	0.72	0.58	0.83	1.10	0.76	0.70	0.70	0.47	0.26	0.25	0.31	0.34	0.14	0.51	0.48
K ₂ O	7.66	6.19	9.23	8.50	8.61	8.48	9.29	9.38	9.18	9.08	9.40	9.66	9.51	9.02	9.04	9.13	9.33
Na ₂ O	0.54	0.60	0.12	0.19	0.54	0.81	0.06	0.00	0.00	0.00	0.09	0.09	0.00	0.00	0.07	0.08	0.15
CaO	0.08	0.00	0.00	0.04	0.22	0.37	0.00	0.00	0.00	0.07	0.00	0.05	0.00	0.00	0.00	0.10	0.08
Total	96.48	96.47	96.48	96.58	95.87	96.63	96.39	95.47	96.57	96.49	96.55	96.58	96.54	96.49	96.51	96.58	96.51

Structural formulae on the basis of 22 oxygens																	
Si	5.68	5.56	5.47	5.88	5.76	5.57	5.54	5.47	5.54	5.58	5.61	5.55	5.59	5.46	5.54	5.55	5.44
Al ^{IV}	2.32	2.44	2.54	2.13	2.24	2.43	2.46	2.53	2.46	2.42	2.39	2.46	2.41	2.54	2.46	2.46	2.56
Al ^{VI}	0.18	0.11	0.47	0.67	0.74	1.05	0.52	0.50	0.51	0.50	0.49	0.41	0.47	0.10	0.16	0.10	0.06
Ti	0.20	0.22	0.43	0.38	0.36	0.07	0.42	0.47	0.44	0.40	0.43	0.43	0.34	0.65	0.55	0.52	0.59
Mg	3.47	3.66	1.36	1.26	1.30	0.71	1.31	1.28	1.34	1.86	1.73	1.81	1.89	2.14	2.26	2.01	1.80
Fe	2.21	2.29	3.31	3.11	2.94	3.63	3.27	3.27	3.25	2.85	2.92	2.95	2.95	2.77	2.72	3.04	3.36
Mn	0.00	0.00	0.10	0.08	0.11	0.15	0.10	0.09	0.09	0.06	0.03	0.03	0.04	0.04	0.02	0.07	0.06
K	1.44	1.16	1.83	1.65	1.68	1.69	1.84	1.86	1.82	1.77	1.83	1.89	1.86	1.76	1.75	1.80	1.87
Na	0.15	0.17	0.04	0.06	0.16	0.25	0.02	0.00	0.00	0.00	0.03	0.03	0.00	0.00	0.02	0.02	0.05
Ca	0.01	0.00	0.00	0.01	0.04	0.06	0.00	0.00	0.00	0.01	0.00	0.01	0.00	0.00	0.00	0.02	0.01
Total	15.66	15.61	15.54	15.21	15.31	15.59	15.48	15.48	15.45	15.44	15.46	15.56	15.56	15.46	15.49	15.57	15.80
X _{Mg}	0.611	0.615	0.291	0.289	0.306	0.163	0.286	0.282	0.291	0.395	0.373	0.381	0.391	0.437	0.454	0.398	0.349

Note: i/Kfs = inclusion in Kfeldspar; i/Pl = inclusion in plagioclase; n = recrystallized grains marking a sub-solidus foliation. Total Fe as FeO. X_{Mg}=Mg/(Fe²⁺+Mg).

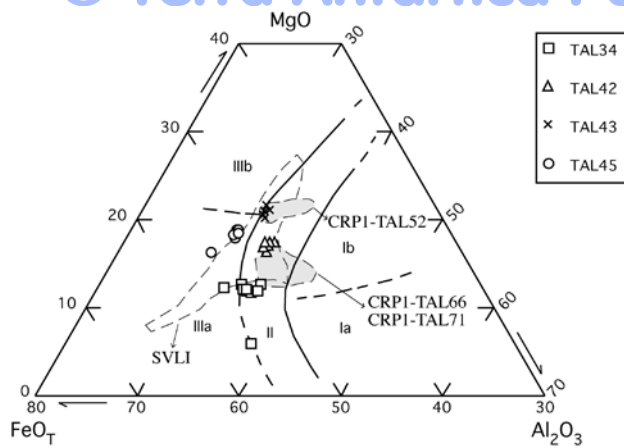


Fig. 5 - Ternary $\text{FeO}_{\text{tot}}\text{-MgO-Al}_2\text{O}_3$ diagram for biotites (after Rossi & Chevremont, 1987) from CRP-2/2A basement clasts. Field I: "Aluminopotassique" association (Ia: type Limousine; Ib: type Guèret); field II: Calcalkaline association; field III: Monzonitic association (IIIa: Fe-potassic; IIIb: Mg-potassic). Outlined field is that of biotite compositions from the calcalkaline South Victoria Land Intrusives (Armenti et al., 1990) on the basis of data reported in Biagini et al. (1991). Compositional fields of biotite from CRP-1 granitoid clasts (Talarico & Sandroni, 1998) are also shown for comparison (CRP1-TAL66: grey biotite monzogranite, 30.62 mbsf; CRP1-TAL71: foliated biotite monzogranite, 40.90 mbsf; CRP1-TAL52: biotite-hornblende granodiorite, 134.71 mbsf).

X_{Mg} ranging from 0.43 (core) to 0.49 (rim). The quartz monzogabbro (CRP2A-TAL43) is characterised by the occurrence of zoned amphiboles with cores of Fe-tschermackitic hornblende ($X_{\text{Mg}}=0.47\text{-}0.49$) and rims consisting of Mg-hornblende ($X_{\text{Mg}}=0.56\text{-}0.57$). Amphibole from the Ca-silicate rock (CRP2A-TAL14) is actinolitic hornblende to actinolite with $X_{\text{Mg}}=0.63\text{-}0.67$. Clinopyroxene (CRP2A-TAL14) is salite and shows very weak intra-crystalline compositional variations from wo49-en35-fs16 (core) to wo49-en33-fs19 (rim).

Feldspars - Representative compositions of plagioclase are listed in table 5. A weak to marked normal zoning was detected in plagioclase from all samples. In undeformed biotite-hornblende monzogranite (CRP2A-TAL45), plagioclase ranges in composition from an46 (core) to an25 (rim). In foliated monzogranite (CRP2A-TAL34), the composition is more sodic, from an33 (core) to an22 (rim) for the phenocrysts, and from an27 to an23 for the recrystallized grains which define the subsolidus foliation. Plagioclases from biotite granodiorite CRP2A-TAL42 show similar compositions ranging from an33 (core) to an28 (rim). In biotite-hornblende quartz monzogabbro (CRP2A-TAL43), plagioclase is characterised by a wider compositional variation in the range from an75 (core) to an52 (rim), and grains occurring as inclusions within K-feldspar are slightly more sodic, from an67-55 (core)

Tab. 4 - Representative chemical analyses of hornblende and clinopyroxene in CRP-2/2A basement clasts.

Oxide (wt%)	Clinoamphibole								Clinopyroxene								
	CRP2A-TAL14			CRP2A-TAL43				CRP2A-TAL45			CRP2A-TAL14						
	1	2	3	1-c	1-r	2-c	2-r	1-c	1-r	2-c	2-r	1-c	1-r	2-c	2-r	3-c	3-r
SiO ₂	53.31	51.39	52.02	41.92	47.20	41.90	48.22	43.58	46.68	44.83	46.21	53.20	53.15	53.02	53.56	52.22	52.42
Al ₂ O ₃	2.31	4.94	3.96	11.36	6.94	11.23	6.47	8.80	6.61	7.97	7.17	0.60	0.49	0.56	0.51	1.07	1.13
TiO ₂	0.00	0.00	0.00	3.25	1.38	2.97	1.05	2.00	1.05	0.45	0.26	0.00	0.00	0.00	0.00	0.00	0.00
FeO	1.55	1.52	2.72	1.99	3.18	2.05	3.17	2.82	3.79	4.08	3.33	0.00	0.00	0.00	0.00	2.09	1.05
MgO	14.28	13.16	14.12	8.67	10.78	8.47	10.89	7.76	9.19	8.13	8.55	11.50	11.38	11.63	11.37	11.47	11.19
FeO	13.51	13.75	12.41	16.27	14.88	17.01	15.24	18.38	16.93	18.16	18.20	10.84	11.36	10.87	10.94	9.42	10.66
MnO	0.11	0.09	0.00	0.49	0.30	0.37	0.31	0.83	0.91	0.79	0.65	0.00	0.09	0.00	0.00	0.07	0.06
CaO	12.19	11.93	11.90	11.36	11.64	11.66	12.06	11.56	11.55	11.84	11.83	23.68	23.48	23.72	23.48	23.29	23.02
Na ₂ O	0.76	0.92	1.01	1.75	0.98	1.64	0.54	1.22	1.13	1.28	1.12	0.19	0.08	0.22	0.15	0.52	0.54
K ₂ O	0.15	0.51	0.38	0.98	0.67	0.96	0.67	1.03	0.75	0.81	0.64	0.00	0.00	0.00	0.00	0.00	0.00
Total	98.17	98.21	98.52	98.04	97.95	98.25	98.63	97.97	98.59	98.35	97.98	100.01	100.03	100.02	100.01	100.15	100.07
Structural formulae on the basis of 23 oxygens.																	
	6 oxygens																
Si	7.71	7.46	7.50	6.32	7.01	6.33	7.10	6.65	7.00	6.81	7.00	2.00	2.01	2.00	2.02	1.97	1.98
Al ^{IV}	0.29	0.54	0.50	1.68	0.99	1.67	0.90	1.35	1.01	1.19	1.01	0.00	0.00	0.00	0.00	0.03	0.02
Al ^{VI}	0.11	0.31	0.17	0.34	0.22	0.33	0.22	0.23	0.16	0.23	0.27	0.03	0.02	0.03	0.02	0.02	0.03
Ti	0.00	0.00	0.00	0.37	0.15	0.34	0.12	0.23	0.12	0.05	0.03	0.00	0.00	0.00	0.00	0.00	0.00
Fe ³⁺	0.17	0.17	0.30	0.23	0.36	0.23	0.35	0.32	0.43	0.47	0.38	0.00	0.00	0.00	0.00	0.06	0.03
Mg	3.08	2.85	3.04	1.95	2.39	1.91	2.39	1.77	2.05	1.84	1.93	0.65	0.64	0.65	0.64	0.65	0.63
Fe ²⁺	1.63	1.67	1.50	2.05	1.85	2.15	1.88	2.34	2.12	2.31	2.30	0.34	0.36	0.34	0.34	0.30	0.34
Mn	0.01	0.01	0.00	0.06	0.04	0.05	0.04	0.11	0.12	0.10	0.08	0.00	0.00	0.00	0.00	0.00	0.00
Ca	1.89	1.86	1.84	1.84	1.85	1.89	1.90	1.89	1.86	1.93	1.92	0.96	0.95	0.96	0.95	0.93	0.93
Na _b	0.21	0.26	0.28	0.51	0.28	0.48	0.16	0.36	0.33	0.38	0.33	0.01	0.01	0.02	0.01	0.04	0.04
K	0.03	0.10	0.07	0.19	0.13	0.19	0.13	0.20	0.14	0.16	0.12	0.00	0.00	0.00	0.00	0.00	0.00
Total	15.13	15.22	15.19	15.54	15.26	15.55	15.18	15.45	15.33	15.46	15.37	3.99	3.99	4.00	3.98	4.00	4.00
X_{Mg}	0.653	0.631	0.670	0.487	0.564	0.470	0.560	0.430	0.492	0.444	0.456	-	-	-	-	-	-
en	-	-	-	-	-	-	-	-	-	-	-	0.333	0.328	0.333	0.332	0.346	0.332
fs	-	-	-	-	-	-	-	-	-	-	-	0.175	0.185	0.174	0.176	0.159	0.179
wo	-	-	-	-	-	-	-	-	-	-	-	0.492	0.487	0.493	0.492	0.495	0.489

Note: c = core composition; r = rim composition.

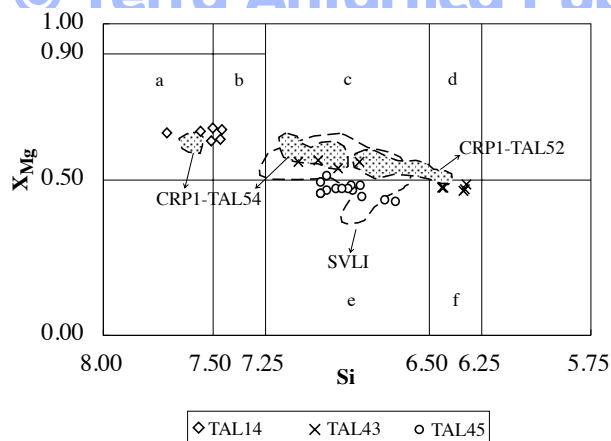


Fig. 6 - Ca-amphibole classification (after Leake, 1978) for CRP-2/2A basement clasts. $(Ca+Na)_B > 1.34$, $(Na+K) < 0.50$. a: actinolite; b: actinolitic hornblende; c: Mg-hornblende; d: tschermackitic hornblende; e: Fe-hornblende; f: Fe-tschermackitic hornblende. The contoured field is that of amphibole compositions from the calcalkaline South Victoria Land Intrusives (Armienti et al., 1990) on the basis of data reported in Biagini et al. (1991). Compositional fields of Ca-amphiboles from CRP-1 basement clasts (Talarico & Sandroni, 1998) are also shown for comparison (CRP1-TAL52: biotite-hornblende granodiorite, 134.71 mbsf; CRP1-TAL54: Ca-silicate rock, 135.33 mbsf).

to an51-46 (rim). Plagioclase from the Ca-silicate rock (CRP2A-TAL14) shows a similarly wide compositional range with labradoritic cores (an62) and andesinic rims (an44-43).

Microperthitic K-feldspar from plutonic samples shows bulk microperthite compositions in the range between or81-ab19 to or84-ab16 (CRP2A-TAL45), or89-ab11 to or92-ab8 (CRP2A-TAL43), and from or84-ab16 (phenocrysts) to or86-ab14 (recrystallized grains) in foliated monzogranite (CRP2A-TAL34). K-feldspar from the Ca-silicate rock (CRP2A-TAL14) ranges in composition from or91-ab9 to or92-ab8.

DISCUSSION AND CONCLUSIONS

Like previous drillholes (MSSTS-1, CIROS-1, CRP-1) on the western edge of the Victoria Land Basin (George, 1989; Barrett et al., 1986; Hambrey et al., 1989; Cape Roberts Science Team, 1998a, 1998d; Talarico & Sandroni, 1998), the CRP-2/2A borehole provides a clear evidence

of a multi-component source for the supply of granule to boulder clasts to the Neogene-Paleogene sedimentary sequences in the McMurdo Sound. This varied provenance closely mirrors the present-day on-shore geological units of the Transantarctic Mountains in southern Victoria Land, which include: 1) granitoid and amphibolite facies metasediments of the Early Paleozoic Ross Orogen; 2) quartz arenites, minor black siltstones and coaly strata of the Devonian-Triassic Beacon Supergroup; 3) dolerite sills and lavas (Kirkpatrick Basalt) of the Jurassic Ferrar Supergroup; and 4) alkaline volcanic rocks of the Cenozoic McMurdo Volcanic Group. Compositional and modal data point to the presence of significant fluctuations in the relative proportions of the main lithologies. In particular they indicate an important lithological change at c. 310 mbsf suggesting a relatively rapid change from a mainly crystalline basement source to one dominated by Ferrar Supergroup lithologies.

They provide clear evidence of an evolving provenance which reflects the unroofing of the deeper basement rocks after an initial phase of erosion which dominantly affected the overlying cover rocks, i.e. the Jurassic basalt and dolerite-intruded Beacon strata.

Preliminary petrographical investigations on CRP-2/2A clasts (Cape Roberts Science Team, 1999) indicated that most of the crystalline basement pebbles from both the Pliocene-Quaternary and Miocene-Oligocene sections, were derived from the Cambro-Ordovician Granite Harbour Intrusive Complex. This complex forms the most extensive outcrops in the local basement (Gunn & Warren, 1962; Allibone et al., 1993a, 1993b; Turnbull et al., 1994). In the region to the west of the Cape Roberts drill sites, between the Mackay Glacier and the central Wright Valley, the Granite Harbour Intrusive Complex consists of several plutons and dyke swarms, which from oldest to youngest (Turnbull et al., 1994), are: Bonney (monzodiorite-granodiorite), Wheeler (quartz diorite to quartz monzodiorite), Valhalla, Suess and St Johns (all granodiorite to granite), biotite granodiorite and granite dikes and plugs, Vanda dyke swarms, and Orestes, Svinford and Harker (all granite). In addition, minor gabbroic to dioritic intrusives occur as either thick dykes (western Clare Range) or small plugs (northwestern St Johns Range, Packard Glacier).

Tab. 5 - Representative plagioclase compositions in CRP-2/2A basement clasts.

	CRP2A-TAL14						CRP2A-TAL34								
	1-c	1-r	2-c	2-r	3-c	3-r	1-c	1-r	2-c	2-r	3-c	3-r	4-n	5-n	6-n
ab	0.529	0.551	0.378	0.546	0.472	0.534	0.640	0.734	0.678	0.762	0.649	0.728	0.739	0.754	0.712
an	0.471	0.438	0.622	0.443	0.517	0.455	0.331	0.235	0.301	0.217	0.320	0.248	0.248	0.230	0.268
or	0.000	0.011	0.000	0.011	0.011	0.011	0.029	0.031	0.021	0.021	0.031	0.024	0.013	0.016	0.020

	CRP2A-TAL42				CRP2A-TAL43				CRP2A-TAL45					
	1-c	1-r	2-c	2-r	1-c	1-r	2-c	2-r	3-c	3-r	1-c	1-r	2-c	2-r
ab	0.632	0.681	0.662	0.699	0.242	0.463	0.317	0.476	0.435	0.530	0.513	0.739	0.620	0.722
an	0.349	0.298	0.325	0.280	0.754	0.522	0.671	0.509	0.549	0.456	0.464	0.235	0.350	0.251
or	0.019	0.021	0.013	0.021	0.004	0.015	0.012	0.015	0.016	0.014	0.023	0.026	0.030	0.027

Note: c = core composition; r = rim composition; n = recrystallized grains marking a sub-solidus foliation; i/Kfs = inclusion in Kfeldspar.

The new petrographic, geochemical and mineral chemistry data provide further evidence for the derivation of most crystalline basement clasts from the locally exposed Granite Harbour Intrusive Complex. Like CRP-1, the ubiquitous occurrence of undeformed biotite±hornblende monzogranite pebbles, in both the Quaternary-Pliocene and Miocene-Oligocene sections, apparently reflects the dominance of these lithologies in the onshore basement.

From both a petrographical and geochemical point of view, these lithologies are indeed akin to the hornblende-biotite and biotite (hornblende-lacking) monzogranites, included in the Dry Valleys 2 (DV2) and Dry Valleys 1b (DV1b) suites, respectively, by Smillie (1992) and Allibone et al. (1993b). In particular, in the region closer to the CRP-2/2A site, biotite monzogranites extensively crop out at Gondola Ridge and in the St Johns Range (they are major constituents of the DV1b - Suess and St Johns Plutons: Allibone et al., 1993b) whereas hornblende-biotite monzogranites are the dominant lithology in the eastern St Johns Range in the Wheeler Valley (the DV2 - discordant Swinford Pluton of Allibone et al., 1993a) as well as at Granite Harbour itself (*e.g.* Lion Island, Graham & Palmer, 1987).

Other, less common and impersistent granitoid varieties forming pebble- to cobble-grade clasts in CRP-2/2A include biotite-hornblende±clinopyroxene granodiorite, grey biotite syenogranite, foliated clinopyroxene-bearing tonalite, biotite-bearing haplogranite, biotite±hornblende-bearing monzogranitic to monzonitic porphyries, and quartz monzogabbro.

Petrographically similar rock types have been reported as minor constituents of the Granite Harbour Igneous Complex in southern Victoria Land. Biotite-hornblende granodiorites have been reported as a major rock type within DV1a plutons of the Dry Valleys-Ferrar region (such as the Bonney Pluton) (Cox, 1993; Allibone et al., 1993a). Biotite syenogranites were reported in both DV2 and DV1b plutons (*cf.* Fig. 8 in Allibone et al., 1993b). Turnbull et al. (1994) report the occurrence of syenogranite in the Harker, Suess and St Johns plutons, whereas tonalites are rare and their nearest outcrops to Cape Roberts are those reported by Smillie (1987) in the cliffs west of the Rhone Glacier (Taylor Valley). Microgranite pebbles are petrographically similar to the leucocratic biotite granite dykes which extensively occur throughout the region (*e.g.* the occurrences reported by Allibone et al., 1993a in the Wright Valley, or by Turnbull et al., 1994 at the eastern margin of the Wheeler Pluton adjacent to the Suess Pluton in the Clare Range). The pebbles of monzogranitic to monzonitic porphyries are likely to have been derived from the younger Vanda felsic porphyry dykes (Allibone et al., 1991), which form intense dike swarms throughout the Mackay Glacier-Askard Range region (Turnbull et al., 1994) and in the Convoy Range, north of the Mackay Glacier (Pocknall et al., 1994). The quartz monzogabbro pebble recalls the gabbroic intrusives which occur in the St Johns Range and form volumetrically minor and scattered sub-concordant dykes and small plugs, such as the Packard Pluton (Turnbull et al., 1994).

Allibone et al. (1993a) interpreted both DV1a and possibly DV1b granitoids as possible correlatives of the

South Victoria Land Intrusives (SVLI) (as defined by Armienti et al., 1990). Compositional data on biotite and hornblende from this metaluminous suite are available for the northernmost segment (between Cape Irizar and the Priestley Glacier, northern Victoria Land - Biagini et al., 1991). As shown in figures 4 and 5, most of the biotite compositions of monzogranite pebbles CRP2A-TAL45 and CRP2A-TAL34, of granodiorite pebble CRP2A-TAL42, and of biotite-hornblende quartz monzogabbro pebble CRP2A-TAL43 plot in the compositional field of biotites from the SVLI. The granodiorite pebble and the biotite-hornblende quartz monzogabbro pebble are also comparable with the SVLI on the basis of hornblende compositions which are typical of the SVLI (Fig. 6). Comparison with the CRP-1 pebbles (Talarico & Sandroni, 1998) shows some overlap between both biotite and hornblende compositions of the biotite-hornblende quartz monzogabbro pebble and those of the biotite-hornblende granodiorite CRP1-TAL52, whereas the CRP-1 monzogranite pebbles (CRP1-TAL66 and CRP1-TAL71) have biotite compositions which are intermediate between those of the two monzogranite pebbles from CRP-2/2A.

The Miocene-Oligocene strata also contain rare pebbles of metamorphic rocks including thinly layered Ca-silicate rocks (clinopyroxene-quartz-plagioclase±calcite-biotite±Ca-amphibole) and two rare occurrences of a biotite orthogneiss (at *c.* 588 mbsf), and of a biotite-clinozoisite schist (at *c.* 599 mbsf). Ca-silicate rocks, characterised by similar mineral assemblages to those found in CRP-2/2A pebbles, and biotite orthogneisses are common lithologies in the amphibolite facies Koettlitz Group (Grindley & Warren, 1964; Williams et al., 1971; Findlay et al., 1984; Allibone, 1992) which, south of Mackay Glacier in the St Johns, Olympus and Clare ranges, forms two NNW- to NW-striking belts, separated by younger granitoid intrusions (Turnbull et al., 1994). Petrographically similar Ca-silicate rock types were also found in CRP-1 core (Talarico & Sandroni, 1998) (*e.g.* sample CRP1-TAL54, 135.33 mbsf, which shows broadly comparable biotite, clinopyroxene and late amphibole compositions to those of CRP2A-TAL14, 88.23 mbsf) (Figs. 4 & 6). The biotite orthogneiss pebble (*c.* 588 mbsf) may have been sourced from the 1 to 100 m thick concordant layers of biotite orthogneisses, which represent a relatively common component within both belts of Koettlitz Group metasedimentary rocks, particularly west of the crest of the St Johns Range (Turnbull et al., 1994). In contrast, the provenance of the biotite-clinozoisite schist pebble remains enigmatic, insofar as similar rock types are at our knowledge currently unknown in southern Victoria Land. According to its mineralogy and microstructural features, both protholith (marl to quartz pelite) and metamorphic grade (low/medium) of this lithology are still potentially consistent with a derivation from the Koettlitz Group, but they would exclude contribution from the predominantly high grade region between the Ferrar and Mackay glaciers (700±50 °C and 4.5±1 kbar, Allibone, 1992).

In conclusion, as in CRP-1, the petrographical, mineral and whole-rock analytical comparison between the CRP-2/2A clasts and lithologies which are extensively exposed in the present-day sector of the Transantarctic

Mountains west and south-west of the Cape Roberts drillsite further supports previous suggestions of a local provenance for basement clasts in the CRP drillsite area.

Having established the provenance of coarse debris contained within the CRP-2/2A succession, it is useful to consider the relationship between the seven petrofacies and the sequence stratigraphy established for the drillhole (Cape Roberts Science Team, 1999; Fielding et al., this volume). Furthermore, recent reinterpretation of seismic reflection data across the drillsites by Henrys et al. (this volume) has allowed a correlation between the sequence stratigraphy for CRP-2/2A and seismic reflector/sequence geometry, which can be used in a preliminary interpretation of geological history of the area. Almost all of the reflectors recognised in Henrys et al.'s reinterpretation correspond to sequence boundaries as interpreted from the core (see Fielding et al., this volume).

Two of the most important surface of discontinuity in CRP-2/2A, at 307 and 443 mbsf (corresponding to the base of Sequences 11 and 18, respectively), also correspond to petrofacies boundaries (P4/P5 and P5/P6, respectively). Other petrofacies boundaries which also correspond to sequence boundaries are top P1 (base Sequence 2), P2/P3 (base Sequence 9), P3/P4 (near base Sequence 10), and P6/P7 (base Sequence 22). Furthermore, every one of the surfaces listed above except the top of P1 (which is too close to the sea-floor to be resolved) corresponds to a reflector recognised in Henrys et al.'s (this volume) reinterpretation of seismic reflection data, with P5/P6 corresponding to the V4/V5 seismic sequence boundary. Two important surfaces recognised in sequence stratigraphic, biostratigraphic and seismic stratigraphic investigations but not reflected in petrofacies boundaries are the base of Sequence 6 at 91 mbsf (the V3/V4 seismic sequence boundary according to Henrys et al., this volume) and the base of Sequence 8 at 130 mbsf (the Miocene/Oligocene unconformity).

Biostratigraphical data and argon-argon age determinations have allowed an estimate of 300 Ka for the interval corresponding to Sequences 9, 10 and 11 (Askin et al., this volume). Significantly, this interval also corresponds to P2 (+ base P1), P3 and P4, respectively. Each of these thick, relatively complete and seismically definable sequences therefore also records a change in sediment provenance, perhaps indicating rearrangement of onshore sediment dispersal systems at each of those boundaries.

ACKNOWLEDGEMENTS

We are very grateful to D.N.B. Skinner and I. Turnbull for reviews and improvements of the manuscript. This work has been carried out as part of the Italian *Programma Nazionale di Ricerche in Antartide*. The Cape Roberts Project was made possible by the resources and close collaboration of the Antarctic programmes of Italy, New Zealand, United States of America, Germany, Australia and Great Britain, with field operation organized by Antarctica New Zealand. We wish to thank those involved in the field phase of the project for their efforts in recovering the core, and the International Steering Committee for access to the core material.

REFERENCES

- Allibone A.H., Forsyth P.J., Sewell R.J., Turnbull I.M. & Bradshaw M.A., 1991. Geology of the Thundergut area, southern Victoria Land, Antarctica, 1:50000. *New Zealand Geological Survey Miscellaneous Geological Map 21* (map and notes). Wellington, New Zealand. Department of Scientific and Industrial Research.
- Allibone A.H., 1992. Low pressure/high temperature metamorphism of Koettlitz Group schists in the Taylor Valley and Ferrar Glacier regions. *New Zealand Journal of Geology and Geophysics*, **35**, 115-127.
- Allibone A.H., Cox S.C., Graham I.J., Smillie R.W., Johnstone R.D., Ellery S.G. & Palmer K., 1993a. Granitoids of the Dry Valleys area, southern Victoria Land, Antarctica: field relationships, and isotopic dating. *New Zealand Journal of Geology and Geophysics*, **36**, 281-291.
- Allibone A.H., Cox S.C. & Smillie R.W., 1993b. Granitoids of the Dry Valleys area, southern Victoria Land: geochemistry and evolution along the early Paleozoic Antarctic Craton margin. *New Zealand Journal of Geology and Geophysics*, **36**, 299-316.
- Armenti P., Ghezzi C., Innocenti F., Manetti P., Rocchi S. & Tonarini S., 1990. Isotope geochemistry and petrology of granitoid suites from Granite Harbour Intrusives of the Wilson Terrane, north Victoria Land, Antarctica. *Eur. J. Mineral.*, **2**, 103-123.
- Barrett P.J., McKelvey B.C. & Walker B.C., 1986. Sand provenance. *DSIR Bulletin*, **237**, 137-144.
- Barrett P.J., Elston D.P., Harwood D.M., McKelvey B.C. & Webb P.N., 1987. Mid-Cenozoic record of glaciation and sea level change on the margin of the Victoria Land basin, Antarctica. *Geology*, **15**, 634-637.
- Biagini R., Di Vincenzo G. & Ghezzi C., 1991. Mineral chemistry of metaluminous granitoids between the David and Campbell Glaciers, Victoria Land (Antarctica). *Mem. Soc. Geol. It.*, **46**, 231-247.
- Cape Roberts Science Team, 1998a. Background to CRP-1, Cape Roberts Project, Antarctica. *Terra Antarctica*, **5**(1), 1-30.
- Cape Roberts Science Team, 1998b. Quaternary Strata in CRP-1, Cape Roberts Project, Antarctica. *Terra Antarctica*, **5**(1), 31-62.
- Cape Roberts Science Team, 1998c. Miocene Strata in CRP-1, Cape Roberts Project, Antarctica. *Terra Antarctica*, **5**(1), 63-124.
- Cape Roberts Science Team, 1998d. Summary Results from CRP-1, Cape Roberts Project, Antarctica. *Terra Antarctica*, **5**(1), 125-138.
- Cape Roberts Science Team, 1999. Studies from Cape Roberts Project. Initial Report on CRP-2/2A, Ross Sea, Antarctica. *Terra Antarctica*, **6**(1/2), 1-173.
- Cooper A.K. & Davey D.J. (eds.), 1987. The Antarctic Continental margin: geology & geophysics of the western Ross Sea. Circum-Pacific Council for Energy & Mineral Resources. *Earth Sciences Series*, **5B**, Houston, Tex.
- Cox S.C., 1993. Inter-related plutonism and deformation in South Victoria Land, Antarctica. *Geological Magazine*, **130**, 1-14.
- Findlay R.H., Skinner D.N.B. & Craw D., 1984. Lithostratigraphy and structure of the Koettlitz Group, McMurdo Sound, Antarctica. *New Zealand Journal of Geology and Geophysics*, **27**, 513-536.
- Franzini M., Leoni L. & Saitta M., 1975. Revisione di una metodologia analitica per fluorescenza X basata sulla correzione completa degli effetti di matrice. *Rend. Soc. It. Min. Petr.*, **31**, 365-378.
- George A., 1989. Sand provenance. *DSIR bulletin*, **245**, 159-167.
- Ghezzi C., Baldelli C., Biagini R., Carmignani L., Di Vincenzo G., Gosso G., Lelli A., Lombardo B., Montrasio A., Pertusati P.C. & Salvini F., 1987. Granitoids from the David Glacier - Aviator Glacier segment of the Transantarctic Mountains, Victoria Land, Antarctica. *Mem. Soc. Geol. It.*, **33**, 143-159.
- Graham I.J. & Palmer K., 1987. New precise Rb-Sr mineral and whole-rock dates for I-type granitoids from Granite Harbour, South Victoria Land, Antarctica. *New Zealand Antarctic Record*, **8**(1), 72-80.
- Grindley G.W. & Warren G., 1964. Stratigraphic nomenclature and correlation in the western part of the Ross Sea. In: Adie R.J. (ed.), *Antarctic geology*, Amsterdam, North Holland Publishing Co., 314-333.
- Gunn B.M. & Warren G., 1962. Geology of Victoria Land between the Mawson and Mulock Glaciers, Antarctica. *New Zealand Geological Survey Bulletin*, **71**.
- Hall K.J., 1989. Clast shape. In: Barrett P.J. (ed.), Antarctic Cenozoic history from the CIROS-1 drillhole, McMurdo Sound. *DSIR Bulletin*, **245**, 63-66.
- Hambrey M.J., Barrett P.J. & Robinson P.H., 1989. Stratigraphy. In: Barrett P.J. (ed.), Antarctic Cenozoic history from the CIROS-1 drillhole, McMurdo Sound. *DSIR Bulletin*, **245**, 23-48.

- Kretz R., 1983. Symbols for rock forming minerals. *Am. Mineral.*, **68**, 277-279.
- Leake B., 1978. Nomenclature of amphiboles. *Mineral. Petrogr. Acta*, **22**, 195-224.
- Leoni L. & Saitta M., 1976. X-ray fluorescence analysis of 29 trace elements in rock and mineral standards. *Rend. Soc. It. Min. Petr.*, **32**, 497-510.
- Papike J.J., Cameron K.L. & Baldwin K., 1974. Amphiboles and clinopyroxenes. Characterization of other than quadrilateral components and estimates of ferric iron from microprobe data. *Geol. Soc. Amer. Abstr. Programs*, **6**, 1053-1054.
- Pocknall D.T., Chinn T.J., Sykes R. & Skinner D.N.B., 1994. Geology of the Convoy Range area, southern Victoria Land, Antarctica. Scale 1:50000. *Institute for Geological & Nuclear Sciences geological map 11*. 1 sheet and 36 p. Institute of Geological & Nuclear Sciences Ltd, Lower Hutt, New Zealand.
- Rossi P. & Chevremont P., 1987. Classification des associations magmatiques granitoides. *Geochronique*, **21**, 14-18.
- Smillie R.W., 1987. Petrological evolution of basement granitoids, southern Victoria Land. *New Zealand Antarctic Record*, **8**(1), 61-71.
- Smillie R.W., 1992. Suite subdivision and petrological evolution of granitoids from the Taylor Valley and Ferrar glacier region, South Victoria Land. *Antarctic Science*, **4**, 71-87.
- Stump E., 1995. *The Ross Orogen of the Transantarctic Mountains*. Cambridge University Press, Cambridge, 249 p.
- Talarico F. & Sandroni S., 1998. Petrography, Mineral Chemistry and Provenance of Basement Clasts in the CRP-1 Drillcore (Victoria Land Basin, Antarctica). *Terra Antarctica*, **5**(3), 601-610.
- Turnbull I.M., Allibone A.H., Forsyth P.J. & Heron D.W., 1994. Geology of the Bull Pass - St Johns Range area, southern Victoria Land, Antarctica. Scale 1:50000. *Institute of Geological & Nuclear Sciences geological map 14*. 1 sheet + 52 p. Institute of Geological & Nuclear Sciences Ltd, Lower Hutt, New Zealand.
- Williams P.F., Hobbs B.E., Vernon R.H. & Anderson D.E., 1971. The structural and metamorphic geology of basement rocks in the McMurdo Sound area, Antarctica. *Journal of the Geological Society of Australia*, **18**, 127-142.